





Cite this: *Chem. Commun.*, 2023, 59, 1773

Received 9th December 2022,  
Accepted 17th January 2023

DOI: 10.1039/d2cc06729c

rsc.li/chemcomm

# An anti-poisoning nanosensor for *in situ* monitoring of intracellular endogenous hydrogen sulfide†

Xi Chen, Wen-Tao Wu, Yu-Ting Jiao, Yi-Ran Kang, Xin-Wei Zhang \* and Wei-Hua Huang \*

**Intracellular H<sub>2</sub>S plays an important regulatory role in cell metabolism. The limited sensing materials and severe sensor passivation hinder its quantification. We functionalized conductive nanowires with MoS<sub>2</sub> and quercetin in a large-scale manner, developed single nanowire sensors with excellent electrocatalytic and anti-poisoning performance, and achieved the accurate quantification of H<sub>2</sub>S within single cells.**

H<sub>2</sub>S is an important endogenous signaling molecule in organisms.<sup>1</sup> As a strong reductive and nucleophilic molecule (H<sub>2</sub>S has lone pair electrons), H<sub>2</sub>S participates in regulating various physiological and pathological processes; for instance, the regulation of redox balance by directly reacting with reactive oxygen/nitrogen species (ROS/RNS) such as H<sub>2</sub>O<sub>2</sub> and NO, promoting vasodilation by persulfidating K<sub>ATP</sub> channels to cause K<sup>+</sup> influx, and so on.<sup>2</sup> Notably, these processes are not only related to the intrinsic chemical properties of H<sub>2</sub>S, but also concentration-dependent.<sup>3</sup> At micromolar concentration, H<sub>2</sub>S generally has a cytoprotective effect. Higher (millimolar) H<sub>2</sub>S tends to be cytotoxic to cells and might lead to inhibition of cell proliferation and pro-inflammatory effects; this is due to the insufficient ATP synthesis and over-expression of pro-inflammatory cytokines, like tumor necrosis factor TNF- $\alpha$ , *etc.*<sup>4</sup>

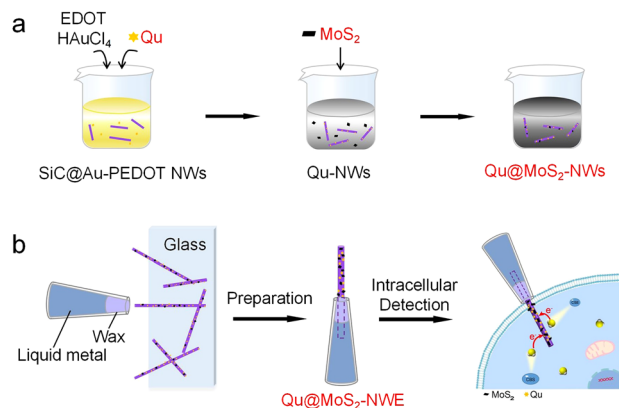
Therefore, the accurate quantification of the concentration of H<sub>2</sub>S facilitates a deeper understanding of its biological significance. Up to now, a variety of analytical methods have been developed for H<sub>2</sub>S detection, including fluorescence,<sup>5</sup> chemiluminescence and electrochemical methods.<sup>6,7</sup> Among them, the electrochemical method stands out because of its quantification ability, high sensitivity and extremely fast response speed, which is very suitable for the detection of H<sub>2</sub>S with considerable reactivity and fast catabolism.<sup>8</sup> Some

micrometer-sized electrodes developed for detecting H<sub>2</sub>S in biological matrices have been reported,<sup>9,10</sup> but most focus on the intercellular H<sub>2</sub>S-mediated physiological processes (neuro-modulation and regulation of vascular tone),<sup>1b,2c</sup> while many important biological effects occurring within cells, such as the effect on mitochondrial ATP and inflammation regulation,<sup>2a,b,4</sup> are less studied. In addition, the synthesis site of H<sub>2</sub>S mainly locates within the cells, including CBS (cystathionine- $\beta$  synthase) and CSE (cystathionine- $\gamma$  lyase) in the cytosol and 3-MST (mercaptopyruvate transferase) in the mitochondrial matrix.<sup>1</sup> These microsensors placed outside the cells cannot easily reflect the accurate concentration of intracellular H<sub>2</sub>S and its biological effects within living cells.<sup>11</sup> Therefore, an *in situ* measurement strategy is indispensable. However, to our best knowledge, the real-time electrochemical detection of intracellular H<sub>2</sub>S has not been reported. Nanoelectrodes provide the possibility for intracellular detection, with their extremely small size and high temporal-spatial resolution, which are suitable for *in situ* analysis within single living cells.<sup>12</sup> Nevertheless, there is an outstanding problem that the electrochemical sensors for detecting H<sub>2</sub>S are easily poisoned owing to the adsorption of the electrooxidation product of H<sub>2</sub>S – elemental sulfur on the electrode surface. This passivation is particularly obvious on the nano-sized electrodes. So, there is an urgent need to develop a robust and anti-sulfur poisoning nanoelectrode to monitor H<sub>2</sub>S within single living cells.

Herein, based on the SiC@Au-PEDOT nanowires with proper aspect ratio and excellent electrical conductivity previously synthesized,<sup>13</sup> we loaded MoS<sub>2</sub> and quercetin (Qu) on these nanowires by a large-scale synthesis method. Here, MoS<sub>2</sub> shows excellent anti-sulfur poisoning and good electrocatalytic performance.<sup>14</sup> Qu, as a kind of catechol derivative, has several hydroxyl groups and a conjugated  $\pi$  system, which might perform as an excellent electron transfer mediator,<sup>15</sup> further enhancing the electrocatalytic performance of MoS<sub>2</sub>. We further fabricated nanoelectrodes with Qu-MoS<sub>2</sub> composite functionalized nanowires. These functionalized nanowire sensors exhibit excellent

College of Chemistry and Molecular Sciences, Wuhan University, Wuhan 430072, China. E-mail: xinweizhang@whu.edu.cn, whhuang@whu.edu.cn

† Electronic supplementary information (ESI) available. See DOI: <https://doi.org/10.1039/d2cc06729c>



**Scheme 1** Illustration of (a) the large-scale synthesis of Qu and MoS<sub>2</sub> co-functionalized nanowires and (b) the preparation of nanosensors for the electrochemical detection of intracellular hydrogen sulfide.

electrocatalytic and anti-sulfur poisoning performance toward H<sub>2</sub>S detection. With such nanosensors, we realized the sensitive and accurate detection of endogenous H<sub>2</sub>S in single living cells.

The synthetic process of the MoS<sub>2</sub>-Qu composite functionalized nanowires is illustrated in Scheme 1. SiC@Au-PEDOT NWs were first synthesized as substrates according to our previous work.<sup>13</sup> 3,4-Ethylenedioxythiophene (EDOT), Qu and H<sub>2</sub>AuCl<sub>4</sub> were then added to the SiC@Au-PEDOT NW dispersion. During the polymerization of EDOT initiated by H<sub>2</sub>AuCl<sub>4</sub>, Qu was simultaneously bound to the generated polyEDOT (PEDOT), thus being stably and uniformly modified on SiC@Au-PEDOT NWs to form Qu-NWs (SiC@Au-PEDOT@Qu nanowires). The negatively charged MoS<sub>2</sub> (zeta potential = -21.3 mV) was added and adsorbed on the positively charged Qu-NWs (zeta potential = +28.4 mV) (Fig. S1, ESI<sup>†</sup>),<sup>16</sup> thus forming the Qu@MoS<sub>2</sub>-NWs (SiC@Au-PEDOT@Qu@MoS<sub>2</sub> nanowires). The morphology of the Qu-NWs and Qu@MoS<sub>2</sub>-NWs was characterized by scanning electron microscopy. Compared with the smooth surface of the Qu-NWs (Fig. 1a), the Qu@MoS<sub>2</sub>-NWs showed a porous structure that was hierarchically assembled by the MoS<sub>2</sub> nanosheets

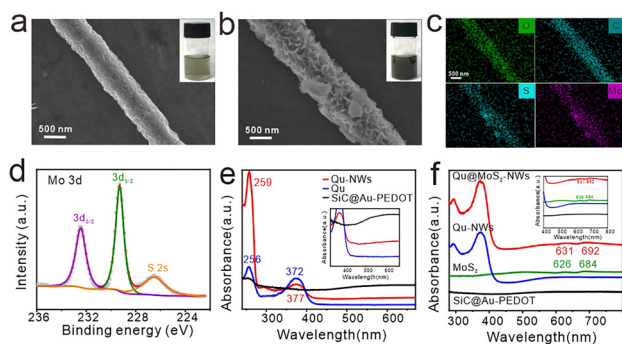


**Fig. 1** (a) SEM image of a Qu-NW (inset: the digital image of the Qu-NW dispersion). (b) SEM image of a Qu@MoS<sub>2</sub>-NW (inset: the digital image of the Qu@MoS<sub>2</sub>-NW dispersion) and (c) corresponding SEM-EDX elemental mapping images. (d) XPS data of Mo 3d states from Qu@MoS<sub>2</sub>-NWs. (e and f) UV/Vis absorption of Qu-NWs, Qu, SiC@Au-PEDOT NWs, Qu@MoS<sub>2</sub>-NWs and MoS<sub>2</sub>.

(Fig. 1b). The energy-dispersive X-ray (EDX) mapping showed that O, C, S and Mo were spread over the prepared nanowires (Fig. 1c). In addition, the X-ray photoelectron spectroscopy results showed the presence of Mo (IV) indicated by the Mo 3d peak at 229.3 and 232.4 eV (Fig. 1d),<sup>17</sup> the Qu was indicated by the O 1s peaks at 533.2 eV (-OH and =O) and 531.3 eV (C-O-C in the pyran functional group) and the PEDOT by the C-O-C bond peak at 532.6 eV (Fig. S2, ESI<sup>†</sup>).<sup>18,19</sup> Moreover, the UV-Vis spectra showed the typical absorption peaks from the benzoyl system (256 nm) and cinnamoyl system (372 nm) in Qu,<sup>20</sup> and the transition peaks of excitons from MoS<sub>2</sub> at 626 nm and 684 nm (Fig. 1e and f).<sup>21</sup> These results confirm the successful preparation of Qu@MoS<sub>2</sub>-NWs.

According to the previously reported protocol for fabricating single nanowire electrodes,<sup>13</sup> we assembled the Qu@MoS<sub>2</sub>-NW to form a nanowire electrode (Qu@MoS<sub>2</sub>-NWE) with a diameter of ~800 nm (Fig. 2a). Its good conductivity was demonstrated by cyclic voltammetry, which was applied on the Qu@MoS<sub>2</sub>-NWE in 1 mM Ru(NH<sub>3</sub>)<sub>6</sub><sup>3+</sup> solution (Fig. S3, ESI<sup>†</sup>). The cyclic voltammogram of Qu@MoS<sub>2</sub>-NWEs in 0.01 M PBS showed a pair of characteristic redox peaks of Qu, which result from the conversion between the phenol and benzoquinone groups (Fig. S4, ESI<sup>†</sup>).<sup>20,22</sup> Moreover, cyclic voltammetry of Qu@MoS<sub>2</sub>-NWE in 1 mM Ru(NH<sub>3</sub>)<sub>6</sub><sup>3+</sup> and 0.01 M PBS was performed for 20 cycles to demonstrate its good stability (Fig. S5 and S6, ESI<sup>†</sup>). This advantage can be attributed to the stable modification of

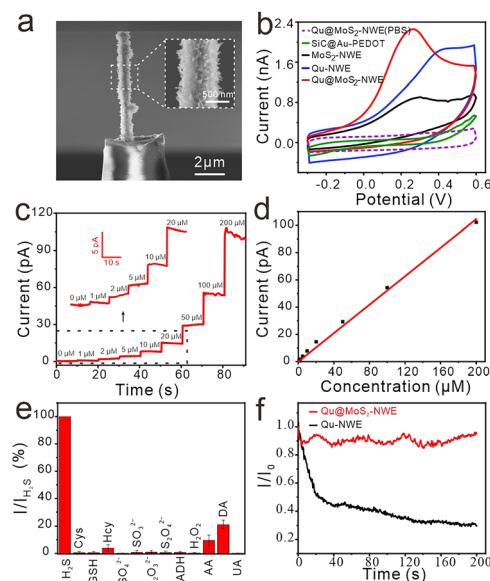


**Fig. 2** (a) SEM image of a Qu@MoS<sub>2</sub>-NWE (inset: An enlarged SEM image showing its detail). (b) CVs recorded for PBS without (dashed line) or with (solid line) 1 mM Na<sub>2</sub>S at the NWE. (c) Amperometric responses of Qu@MoS<sub>2</sub>-NWE to a series of increasing Na<sub>2</sub>S concentrations at the potential of +300 mV (vs. Ag/AgCl) and (d) the corresponding calibration curves. (e) Selectivity test of the Qu@MoS<sub>2</sub>-NWE towards common interferents at +300 mV (vs. Ag/AgCl); 200 μM for cysteine (Cys), 10 mM for glutathione (GSH), and 50 μM for others. (f) Amperometric current response toward 50 μM Na<sub>2</sub>S recorded with the Qu-NWE (black curve) and Qu@MoS<sub>2</sub>-NWE (red curve) at +300 mV (vs. Ag/AgCl), where *I*<sub>0</sub> and *I* are the current values at the starting time and given time, respectively.

Qu and the strong electrostatic interaction between the Qu-NWs and MoS<sub>2</sub>.

The electrocatalytic ability of the Qu@MoS<sub>2</sub>-NWEs for H<sub>2</sub>S was further assessed. 1 mM Na<sub>2</sub>S solution was used to prepare the standard solution, which can instantaneously generate HS<sup>−</sup> and S<sup>2−</sup> at the physiological pH. Its electrochemical oxidation behavior at the SiC@Au–PEDOT NWE, Qu-NWE, MoS<sub>2</sub>-NWE and Qu@MoS<sub>2</sub>-NWE was examined by cyclic voltammetry (Fig. 2b). It could be seen that the SiC@Au–PEDOT NWE only exhibited a weak upturned current response, while the Qu@MoS<sub>2</sub>-NWE exhibited a more significant catalytic performance, which started oxidizing Na<sub>2</sub>S around −0.1 V and reached a maximum oxidation current around 0.25 V. Compared with the Qu-NWE and MoS<sub>2</sub>-NWE, the Qu@MoS<sub>2</sub>-NWE possesses obviously higher peak current and lower peak potential for oxidation of Na<sub>2</sub>S. These results indicated that the MoS<sub>2</sub> and Qu composites had a better electrocatalytic ability than individual MoS<sub>2</sub> or Qu. This excellent electrochemical performance might be attributed to a larger specific area of the porous structure as well as the synergistic effect of MoS<sub>2</sub> and Qu. Specifically, the MoS<sub>2</sub> efficiently catalyzed the oxidation of Na<sub>2</sub>S, while the Qu acted as a good electron transfer mediator which increased the charge transfer rate. The detection ability of the Qu@MoS<sub>2</sub>-NWE towards H<sub>2</sub>S was further examined by the amperometric method, and a good linear relationship was obtained between the oxidation peak currents and the Na<sub>2</sub>S concentration from 1 μM to 200 μM (Fig. 2c and d). The detection limit was calculated to be about 300 nM (S/N = 3, R<sup>2</sup> = 0.997). Furthermore, Qu@MoS<sub>2</sub>-NWE exhibited an excellent selectivity toward Na<sub>2</sub>S compared to some interferents, including sulfur-containing reagents and other common biomolecules (Fig. 2e). As mentioned above, during the electrochemical detection of Na<sub>2</sub>S, the deposited sulfur usually passivates the electrode active surface and greatly decreases the sensitivity. But the MoS<sub>2</sub> with good sulfur tolerance might present a high anti-poisoning performance. To verify this ability of MoS<sub>2</sub>, we recorded amperometric responses of 50 μM Na<sub>2</sub>S (this level is higher than the endogenous H<sub>2</sub>S concentration of *ca.* 15 μM in MCF-7 cell lines<sup>23</sup>) at the Qu@MoS<sub>2</sub>-NWE and Qu-NWE (*E* = 300 mV). The Qu@MoS<sub>2</sub>-NWE could output a stable current response to 50 μM Na<sub>2</sub>S, whereas the Qu-NWE showed a decreasing current response (Fig. 2f and Fig. S7 and S8, ESI†). Furthermore, the average normalized current (*I*/*I*<sub>0</sub>) recorded at Qu@MoS<sub>2</sub>-NWEs at 200 s was 93%, which was much higher than 30% compared with that at Qu-NWEs (Fig. S9, ESI†). These results confirmed that MoS<sub>2</sub> presents a good anti-sulfur poisoning performance, which may be attributed to the repulsive force between the sulfur atom layers of MoS<sub>2</sub> and the elemental sulfur produced by H<sub>2</sub>S oxidation. When elemental sulfur was produced on the electrode surface, it may be repelled by the sulfur layers of MoS<sub>2</sub> and preferably escape to the bulk solution instead of depositing on the electrode surface.<sup>14</sup>

H<sub>2</sub>S is an important signaling molecule within cells and plays concentration-dependent regulation roles in intracellular metabolism. Herein, we applied Qu@MoS<sub>2</sub>-NWEs for the

quantitative monitoring of H<sub>2</sub>S in living cells. The capability of Qu@MoS<sub>2</sub>-NWEs for intracellular detection was first evaluated. Due to the nano-size and good mechanical properties of the Qu@MoS<sub>2</sub>-NWEs, they could easily penetrate through the cell membrane and be tightly sealed by the membrane. This process was confirmed by monitoring the limiting reduction currents of Ru(NH<sub>3</sub>)<sub>6</sub><sup>3+</sup> (1 mM in the extracellular bath solution), which can be reduced at the electrode but cannot cross the cellular membranes. As the depth of NWE insertion into cells increased, the limiting reduction current of Ru(NH<sub>3</sub>)<sub>6</sub><sup>3+</sup> decreased correspondingly, and also almost recovered (~95%) when the electrode was completely withdrawn from the cells (Fig. S10a, ESI†).<sup>24</sup> Meanwhile, the high viability of the penetrated cells was proved by the fluorescence staining with calcein-AM and propidium iodide (PI), indicating that the insertion of Qu@MoS<sub>2</sub>-NWEs caused no significant damage to the cells (Fig. S10b, ESI†). These results demonstrated that Qu@MoS<sub>2</sub>-NWEs were suitable for intracellular detection.

For intracellular H<sub>2</sub>S detection, we first applied a constant potential of 300 mV to the Qu@MoS<sub>2</sub>-NWEs and then positioned the Qu@MoS<sub>2</sub>-NWEs in contact with the MCF-7 cell membrane. It could be seen that there were no amperometric responses when the NWEs were outside the cells (amperometric trace on the left of the blue line in Fig. 3b). When the NWEs were completely inserted, weaker amperometric response signals were detected in the cells without any treatment. When the cells were treated with 10 mM Cys (the main substrate of the H<sub>2</sub>S synthesis, Fig. 3a) for 1 h to upregulate the intracellular H<sub>2</sub>S levels, an obviously elevated amperometric response was recorded. Whereas when the cells were pre-treated with 1 mM aminooxy acetic acid (AOAA, an inhibitor of PLP (pyridoxal-5-phosphate monohydrate)-dependent enzymes such as CBS and CSE) for 1 h,<sup>25</sup> and subsequently treated with 10 mM Cys for 1 h, significantly smaller amperometric responses were detected (Fig. 3b). By integrating the

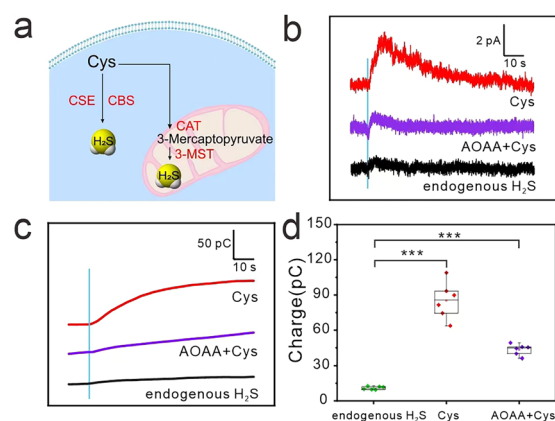


**Fig. 3** (a) Illustration of the synthetic pathway of H<sub>2</sub>S in cells. (b–d) Amperometric traces obtained from MCF-7 cells with Cys (10 mM) incubation (red curve), with AOAA (1 mM) and Cys (10 mM) incubation (purple curve) and without treatment (back curve), and the corresponding charge curves (c) and charge statistics (d, *n* = 6, \*\*\**P* < 0.001). The blue line indicates the moment of Qu@MoS<sub>2</sub>-NWE insertion, and the potential for intracellular H<sub>2</sub>S measurements was +300 mV (vs. Ag/AgCl).

current over the time, the corresponding charges are shown in Fig. 3c. The statistical charge data are illustrated in Fig. 3d, and it can be seen that the total charge generated by intracellular endogenous  $\text{H}_2\text{S}$  oxidation was  $11.8 \pm 1.8$  pC, which was lower than the 74.0 pC in Cys-treated cells and 31.6 pC in AOAA + Cys-treated cells.

Moreover, according to Faraday's law and the volume of a cell (the average diameter of spherical MCF-7 cells measured as  $\sim 9$   $\mu\text{m}$ ), the endogenous  $\text{H}_2\text{S}$  concentration in a single MCF-7 cell was calculated to be  $20.4 \pm 3.1$   $\mu\text{M}$ . At this concentration,  $\text{H}_2\text{S}$  is considered physiologically beneficial, and acts as an electron donor to stimulate mitochondrial electron transport and promote ATP synthesis, thus providing energy for the proliferation and migration of MCF-7 cells.<sup>26</sup> In addition, since the electrode could output a stable current response to 50  $\mu\text{M}$   $\text{Na}_2\text{S}$  for 200 s, which was longer than the acquisition time ( $\sim 100$  s) of intracellular detection, the anti-sulfur poisoning performance of the Qu@MoS<sub>2</sub>-NWEs ensured the accurate quantification of intracellular endogenous  $\text{H}_2\text{S}$ .

In conclusion, we prepared a novel single nanowire sensor by versatile and facile co-modification of MoS<sub>2</sub> and Qu on nanowires. The excellent catalytic and good anti-sulfur poisoning properties of the MoS<sub>2</sub>-Qu composite endow the nanowire electrodes with outstanding  $\text{H}_2\text{S}$  sensing performance, thus ensuring the accurate quantification of endogenous  $\text{H}_2\text{S}$  in MCF-7 cells. The measured concentration of endogenous  $\text{H}_2\text{S}$  in MCF-7 cells is approximately 20  $\mu\text{M}$ , which was considered to be physiologically beneficial. The nanowire sensor would be an effective tool for the accurate quantification of  $\text{H}_2\text{S}$  levels in various pathological conditions such as cancer, neurodegenerative diseases and cardiovascular diseases, which will be of great significance for better understanding the biphasic biological roles of  $\text{H}_2\text{S}$  in these processes.

We gratefully acknowledge financial support from the National Natural Science Foundation of China (Grants 21725504, 22090050, 22090051, and 21721005).

## Conflicts of interest

There are no conflicts to declare.

## Notes and references

- (a) A. Aroca, C. Gotor, D. C. Bassham and L. C. J. A. Romero, *Antioxidants*, 2020, **9**, 621; (b) H. Kimura, N. Shibuya and Y. Kimura, *Antioxid. Redox Signaling*, 2012, **17**, 45–57.
- (a) M. R. Filipovic, J. Zivanovic, B. Alvarez and R. Banerjee, *Chem. Rev.*, 2018, **118**, 1253–1337; (b) L. Li, P. Rose and P. K. Moore, *Annu. Rev. Pharmacol. Toxicol.*, 2011, **51**, 169–187; (c) N. Skovgaard, A. Gouliaev, M. Aalling and U. Simonsen, *Curr. Pharm. Biotechnol.*, 2011, **12**, 1385–1393.
- B. D. Paul, S. H. Snyder and K. Kashfi, *Redox Biol.*, 2021, **38**, 101772.
- (a) C. Szabo, *Cells*, 2021, **10**, 220; (b) C. Szabo, *Nat. Rev. Drug Discovery*, 2007, **6**, 917–935; (c) C. Szabo, C. Ransy, K. Módis, M. Andriamihaja, B. Murghes, C. Coletta, G. Olah, K. Yanagi and F. Bouillaud, *Br. J. Pharmacol.*, 2014, **171**, 2099–2122.
- (a) Y. Chen, C. Zhu, Z. Yang, J. Chen, Y. He, Y. Jiao, W. He, L. Qiu, J. Cen and Z. Guo, *Angew. Chem., Int. Ed.*, 2013, **52**, 1688–1691; (b) Y. Qian, J. Karpus, O. Kabil, S.-Y. Zhang, H.-L. Zhu, R. Banerjee, J. Zhao and C. He, *Nat. Commun.*, 2011, **2**, 495.
- (a) B. Ke, W. Wu, W. Liu, H. Liang, D. Gong, X. Hu and M. Li, *Anal. Chem.*, 2016, **88**, 592–595; (b) T. S. Bailey and M. D. Pluth, *J. Am. Chem. Soc.*, 2013, **135**, 16697–16704.
- (a) S. Wang, X. Liu and M. Zhang, *Anal. Chem.*, 2017, **89**, 5382–5388; (b) K. S. Shalini Devi and A. Senthil Kumar, *Analyst*, 2018, **143**, 3114–3123; (c) Y. Qian, L. Zhang and Y. Tian, *Anal. Chem.*, 2022, **94**, 1447–1455.
- J. Myszkowska, I. Derevenkov, S. V. Makarov, U. Spiekerkoetter and L. Hannibal, *Antioxidants*, 2021, **10**, 1065.
- X.-B. Hu, Y.-L. Liu, H.-W. Zhang, C. Xiao, Y. Qin, H.-H. Duo, J.-Q. Xu, S. Guo, D.-W. Pang and W.-H. Huang, *ChemElectroChem*, 2016, **3**, 1998–2002.
- H. Dong, Q. Zhou, L. Zhang and Y. Tian, *Angew. Chem., Int. Ed.*, 2019, **58**, 13948–13953.
- F.-S. Quan and G.-J. Lee, *BioMed Res. Int.*, 2021, 5473965.
- (a) N. T. N. Phan, X. Li and A. G. Ewing, *Nat. Rev. Chem.*, 2017, **1**, 0048; (b) W. Wang, S.-H. Zhang, L.-M. Li, Z.-L. Wang, J.-K. Cheng and W.-H. Huang, *Anal. Bioanal. Chem.*, 2009, **394**, 17–32; (c) X.-W. Zhang, A. Hatamie and A. G. Ewing, *Curr. Opin. Electrochem.*, 2020, **22**, 94–101; (d) K. Ino, Y. Nashimoto, N. Taira, J. R. Azcon and H. Shiku, *Electroanalysis*, 2018, **30**, 2195–2209.
- W.-T. Wu, H. Jiang, Y.-T. Qi, W.-T. Fan, J. Yan, Y.-L. Liu and W.-H. Huang, *Angew. Chem., Int. Ed.*, 2021, **60**, 19337–19343.
- (a) N. Jeromiyas, V. Mani, P.-C. Chang, C.-H. Huang, K. N. Salama and S.-T. Huang, *Sens. Actuators, B*, 2021, **326**, 128844; (b) V. Mani, S. Selvaraj, N. Jeromiyas, S.-T. Huang, H. Ikeda, Y. Hayakawa, S. Ponnusamy, C. Muthamizhchelvan and K. N. Salama, *J. Mater. Chem. B*, 2020, **8**, 7453–7465.
- L. V. da Silva, A. K. A. de Almeida, J. A. Xavier, C. B. Lopes, F. d. A. d. S. Silva, P. R. Lima, N. D. dos Santos, L. T. Kubota and M. O. F. Goulart, *J. Electroanal. Chem.*, 2018, **827**, 230–252.
- S. Khaledian, D. Kahrizi, S. Tofik Jalal Balaky, E. Arkan, M. Abdoli and F. Martinez, *J. Mol. Liq.*, 2021, **334**, 115989.
- H. Nan, Z. Wang, W. Wang, Z. Liang, Y. Lu, Q. Chen, D. He, P. Tan, F. Miao, X. Wang, J. Wang and Z. Ni, *ACS Nano*, 2014, **8**, 5738–5745.
- K. Bourhis, S. Blanc, C. Mathe, J.-C. Dupin and C. Vieillescazes, *Appl. Clay Sci.*, 2011, **53**, 598–607.
- Z. Liu, J. Xu, R. Yue, T. Yang and L. Gao, *Electrochim. Acta*, 2016, **196**, 1–12.
- W. Liu and R. Guo, *J. Colloid Interface Sci.*, 2006, **302**, 625–632.
- T. Chen, H. Zou, X. Wu, C. Liu, B. Situ, L. Zheng and G. Yang, *ACS Appl. Mater. Interfaces*, 2018, **10**, 12453–12462.
- Y. Dilgin, B. Kizilkaya, B. Ertek, N. Eren and D. G. Dilgin, *Talanta*, 2012, **89**, 490–495.
- M. Zuo, Q. Duan, C. Li, J. Ge, Q. Wang, Z. Li and Z. Liu, *Anal. Chem.*, 2021, **93**, 5635–5643.
- Y. Wang, J.-M. Noël, J. Velmurugan, W. Nogala, M. V. Mirkin, C. Lu, M. Guille Collignon, F. Lemaître and C. Amatore, *Proc. Nat. Acad. Sci.*, 2012, **109**, 11534–11539; X.-W. Zhang, Q.-F. Qiu, H. Jiang, F.-L. Zhang, Y.-L. Liu, C. Amatore and W.-H. Huang, *Angew. Chem., Int. Ed.*, 2017, **56**, 12997.
- A. Asimakopoulou, P. Panopoulos, C. T. Chasapis, C. Coletta, Z. Zhou, G. Cirino, A. Giannis, C. Szabo, G. A. Spyroulias and A. Papapetropoulos, *Br. J. Pharmacol.*, 2013, **169**, 922–932.
- C. Szabo, C. Coletta, C. Chao, K. Módis, B. Szczesny, A. Papapetropoulos and M. R. Hellmich, *Proc. Nat. Acad. Sci.*, 2013, **110**, 12474–12479.